Elsevier Editorial System(tm) for Journal of Magnesium and Alloys

Manuscript Draft

Manuscript Number: JMA-D-17-00017

Title: Effects of Mg2+ interstitial ion on the properties of Mg0.5+x/2Si2-xAlx(PO4)3 ceramic electrolytes

Article Type: Original Research Article

Keywords: Ceramic, electrolyte, Mg electrolyte, interstitial ion, Nasicon

Corresponding Author: Dr. Adnan SBRS, PhD

Corresponding Author's Institution: University of malaya

First Author: Adnan SBRS, PhD

Order of Authors: Adnan SBRS, PhD

Abstract: Nasicon type, Mg0.5+x/2Si2-xAlx(PO4)3 was synthesized using citric acid assisted sol-gel method. The X-ray diffraction was applied to investigate the effect of extra Mg2+ interstitial ion on the phase, unit cell parameters and structure of the samples. The Mg0.625Si1.75Al0.25(PO4)3 sample exhibited highest bulk conductivity value of 1.54 ×10-4 S cm-1 at ambient temperature. The frequency dependence of the σac of these ceramic electrolytes follows the universal power law variation, σac (ω) = σo + Aωα. The conductivity parameters such as hopping frequencies, charge carrier concentration and mobile ion concentration proved that the increase in conductivity with x was due to the existing of Mg2+ interstitial ion. The experiment results also revealed that the dielectric constant and dielectric loss decreased with frequency. The Mg0.625Si1.75Al0.25(PO4)3 was found to be electrochemically stable up to 2.51 V at ambient temperature.

Suggested Reviewers: Larbi Zerroual
Zerroual@yahoo.fr
He experts in this area

Ri hanum yahya
rihanum43@salam.uitm.edu.my
she experts in this area

Nur Amalina Mustaffa
nuramalina@salam.uitm.edu.my
she experts in this area

Opposed Reviewers:

Effects of Mg^{2+} interstitial ion on the properties of $Mg_{0.5+x/2}Si_{2-x}Al_x(PO_4)_3$ ceramic electrolytes

Z.A. Halim[1], S.B.R.S Adnan[2] and N.S. Mohamed[2]*

[1]Institute of Graduate Studies, University of Malaya, 50603 Kuala Lumpur, Malaysia

[2]Centre for Foundation Studies in Science, University of Malaya, 50603 Kuala Lumpur, Malaysia
Email: syed_bahari@um.edu.my*

ABSTRACT

Nasicon type, $Mg_{0.5+x/2}Si_{2-x}Al_x(PO_4)_3$ was synthesized using citric acid assisted sol-gel method. The X-ray diffraction was applied to investigate the effect of extra Mg^{2+} interstitial ion on the phase, unit cell parameters and structure of the samples. The $Mg_{0.625}Si_{1.75}Al_{0.25}(PO_4)_3$ sample exhibited highest bulk conductivity value of 1.54×10^{-4} S cm^{-1} at ambient temperature. The frequency dependence of the σ_{ac} of these ceramic electrolytes follows the universal power law variation, $\sigma_{ac}(\omega) = \sigma_o + A\omega^{\alpha}$. The conductivity parameters such as hopping frequencies, charge carrier concentration and mobile ion concentration proved that the increase in conductivity with *x* was due to the existing of Mg^{2+} interstitial ion. The experiment results also revealed that the dielectric constant and dielectric loss decreased with frequency. The $Mg_{0.625}Si_{1.75}Al_{0.25}(PO_4)_3$ was found to be electrochemically stable up to 2.51 V at ambient temperature.

Keywords : Ceramic, electrolyte, Mg electrolyte, interstitial ion, Nasicon

1. INTRODUCTION

Magnesium batteries have recently attracted great interest due to their high energy density and environmentally friendly components [1]. Theoretically, these Mg batteries can offer high volumetric specific capacity compared to lithium (3833 mAh/cm3 for Mg vs. 2046 mAh/cm^3 for Li) [1]. Considering all these aspects, it is clear that magnesium battery systems could offer a

significantly cheaper, safer and better-performing battery option in contrast to lithium [1]. Despite these attractive attributes of Mg batteries, there are several challenges pertaining to the use of cathodes, electrolytes and anodes. With respect to electrolytes, the magnesium electrolytes's compound has to show high ionic conductivity, large enough interstitial void and high structural stability based on 3D framework [2].

There is only a limited number of works on the use of magnesium as an electrolyte in magnesium batteries. This is may due to the (i) difficulty for the divalent Mg-ion to diffuse in solid electrolytes compared to the monovalent Li-ion, (ii) narrow electrical window of electrolytes used for Mg-ion electrochemical activity and finally (iii) relatively low specific energy of magnesium ion batteries compared to its lithium counterpart [3]. Anuar et al started to synthesize magnesium electrolytes based on Nasicon type, $Mg_{0.5}Zr_2\ (PO_4)_3$ [2]. However, the Nasicon's lattice size was too large making the structure unstable. To overcome this problem, the authors replaced Zr^{4+} with Si^{4+} as reported in an early paper [4] in order to reduce the lattice size of the Nasicon's structural. The conductivity of $Mg_{0.5}Si_2(PO_4)_3$ solid electrolytes is an order of magnitude higher than the $Mg_{0.5}Zr_2(PO_4)_3$ solid electrolytes.

The conductivity of the Nasicon materials can also be improved by modifying their unit cell dimension and ion concentration (interstitial ion and vacant site)[5][6][7]. Therefore, in the effort to enhance the conductivity of previous $Mg_{0.5}Si_2(PO_4)_3$ compound, the authors substituted Al^{3+} at the Si^{4+} site ($Si^{4+} \leftrightarrow Al^{3+} + 1/2Mg^{2+}$) in order to create Mg^{2+} interstitial ions in the lattice site to obtain compounds with formula $Mg_{0.5+x/2}Si_{2-x}Al_x(PO_4)_3$. To the best of our knowledge, no studies on the use of Al^{3+} as conductivity enhancing agent in the $Mg_{0.5}Si_2(PO_4)_3$ compound have been reported in the literature.

In this paper, the effects of Mg^{2+} interstitial ion on the thermal, structural, electrical and electrochemical properties of the $Mg_{0.5+x/2}Si_{2-x}Al_x$ $(PO_4)_3$ compound prepared by the sol gel method were investigated. For this purpose, the $Mg_{0.5+x/2}Si_{2-x}Al_x(PO_4)_3$ samples were subjected to X-ray diffraction, scanning electron microscopy, impedance spectroscopy and linear sweep Voltammetry analysis.

2. EXPERIMENTAL PROCEDURE

2.1 Synthesis of $Mg_{0.5+x/2}Si_{2-x}Al_x(PO_4)_3$ samples

For sample preparation, magnesium acetate tethrahydrate, tetraethyl orthoslilicate, aluminium acetate and ammonium phosphate monobasic (H_6NO_4P) were used as the starting materials Meanwhile citric acid ($C_6H_8O_7$) was employed as the chelating agent. The molar ratio of Mg:Si:Al:P:O was determined based on the stoichiometric formula of $Mg_{0.5+x/2}Si_{2-x}Al_x(PO_4)_3$ with x = 0.10, 0.15, 0.20 and 0.25. The starting materials were first dissolved separately in distilled water and then stirred for 1 hour under magnetic stirring at a temperature of 30^{o}C. All of the solutions were mixed together and stirred in a reflux system at 70^{o}C for 24 hours to form a homogeneous solution. The solution was taken out and then evaporated for at least 7 hours under magnetic stirring at 80^{o}C. The resulting wet gel was dried in a vacuum oven at 150^{o}C for 24 hours to remove water particles and resistance organic. The obtained powder was heated at 400^{o}C for 4 h to remove ammonium and acetate groups. The powder samples were later annealed at sintering temperatures of 800^{o}C for 4 h.

2.2 Characterization techniques

The X-ray powder diffraction analysis was carried out using PANalytical-X'pert^3 X-ray diffractometer with Cu-Kα radiation of wavelength of 1.5406Å in 2θ range from 10^o to 40^o. Then, the monoclinic lattice parameters of the samples were calculated using the formula [8]:

$$\frac{1}{d^2} = \frac{1}{\sin^2\beta}\left(\frac{h^2}{a^2} + \frac{k^2\sin^2\beta}{b^2} + \frac{l^2}{c^2} - \frac{2hl\cos\beta}{ac}\right) \quad (1)$$

and

$$d = \frac{\lambda}{2\sin\theta} \quad (2)$$

Where d is the distance between crystal planes of *(hkl)*, λ is the X-ray wavelength, θ is the diffraction angle of crystal plane , *hkl* is the crystal index, *a*, *b* and *c* are the lattice parameters and β is the angle between a and c. A Zeiss-Evo MA10 scanning electron microscope was used to conduct morphological analysis of the $Mg_{0.5+x/2}Si_{2-x}Al_x(PO_4)_3$ powders. The particle size information of the ceramic samples was acquired using FRITSCH-Analysette 22 NanoTec laser particle sizer at room temperature. Complex impedance parameters (i.e. impedance and phase angle parameters) were measured with a computer-controlled SOLATRON 1260 impedance analyser The samples were sandwiched between platinum electrode which served as non-blocking electrodes in a frequency range from 0.1 to 10^6 Hz. The total conductivity, σ_t (bulk conductivity, σ_b + grain boundary conductivity, σ_{gb}) which represents the direct current (dc) conductivity in the ceramic sample was calculated using the equation:

$$\frac{1}{\sigma_t} = \frac{1}{\sigma_b} + \frac{1}{\sigma_{gb}} \quad (3)$$

where $\sigma_b = \frac{d}{AR_b}$ and $\sigma_{gb} = \frac{d}{AR_{gb}}$

In these equations, *d* is the sample thickness, *A* is the cross-sectional area of the sample, R_b is the bulk resistance and R_{gb} is the grain boundary resistance. Ac conductivity has been evaluated from dielectric data in accordance with the relation:

$$\sigma_{ac} = \omega \varepsilon_o \varepsilon'' \tan\delta \quad (4)$$

where ε_o is the permittivity of the free space (8.854×10^{-14} F cm^{-1}), $\omega = 2\pi f$, ε'' is the dielectric loss and $\tan\delta$ is the loss tangent factor. The electrochemical stability of the studied samples was evaluated by LSV using Wnatech ZIVE MP2 multichannel electrochemical workstation. The samples were placed between two stainless steel blocking electrodes and a potential current of 0.5 V was applied in order to polarize them. The current was then monitored as a function of time until it reached a steady state condition.

3. RESULT AND DISCUSSION

Presented in Figure 1 is the XRD spectra of $Mg_{0.5+x/2}Si_{2-x}Al_x(PO_4)_3$ (x = 0.10, 0.15, 0.20 and 0.25) samples. All of the samples exhibit sharp diffraction peaks attributed only to $Mg_{0.5+x/2}Si_{2-x}Al_x(PO_4)_3$ which proves that all compounds were pure. The XRD spectra of the samples were indexed to monoclinic structure with a space group of $P12_1/c1$. All of the $Mg_{0.5+x/2}Si_{2-x}Al_x(PO_4)_3$ peaks are sharp and well defined, indicating that the samples are generally well crystallized.

There are synchronizations between the result of lattice parameters, crystallite size, density and volume of the samples which increase with the increase of *x* as shown in Table 1. The increase in the unit cell volume is attributed to the larger atomic size of Al^{3+} than Si^{4+} and due to the existing of additional interstitial Mg^{2+} ion after successfully partial substituted process in the samples [9]. Meanwhile, the increase in the crystallite size is due to the grain growth process on the samples [10, 11]. This confirm that the Mg-ion interstitial affected the structures of the ceramic compounds.

SEM micrographs and particle size distributions of the $Mg_{0.5+x/2}Si_{2-x}Al_x(PO_4)_3$ (x = 0.10, 0.15, 0.20 and 0.25) samples are displayed in Figure 2 and Figure 3 respectively. SEM micrographs show that the particle size increases from x = 0.10 to x = 0.25. Meanwhile, Figure 3 clearly shown that the size of the particles in $Mg_{0.5+x/2}Si_{2-x}Al_x(PO_4)_3$ samples increases with the increase of x. As the x increases, the average size of the particles in the $Mg_{0.5+x/2}Si_{2-x}Al_x(PO_4)_3$ samples increases from 35.7 μm to 58.9 μm.

The impedance plots of the $Mg_{0.5+x/2}Si_{2-x}Al_x(PO_4)_3$ (x = 0.10, 0.15, 0.20 and 0.25) samples are shown in Figure 4. The impedance plot for every sample consists of two overlapping semicircles with a titled spike at low frequency region. The high-frequency semicircle is ascribed to bulk response with its intercept at the x-axis attributed to bulk resistance, R_b, while the middle frequency semicircle is associated to grain boundary response with its intercept at the x-axis corresponding to grain boundary resistance, R_{gb} [12]. On the other hand, the spike that can be clearly seen at the low frequency region of the spectra indicates the effects of electrode polarization as a result of accumulation of ions between electrode and samples [13].

The complex impedance data obtained experimentally for the $Mg_{0.5+x/2}Si_{2-x}Al_x(PO_4)_3$ (x = 0.10, 0.15, 0.20 and 0.25) samples at room temperature may be approximately denoted by the

impedance of an equivalent circuit consisting of bulk resistance (R_b), grain boundary resistance (R_{gb}), bulk, C_b (CPE), grain boundary capacitance C_{gb} (CPE) and CPE blocking electrode as shown in Figure 5. Table 2 lists direct current conductivity values of all $Mg_{0.5+x/2}Si_{2-x}Al_x(PO_4)_3$ samples calculated using equation 3. The conductivity increases consistently from $x = 0.10$ to $x = 0.25$. The sample with $x = 0.25$ gives the highest bulk conductivity with value of 1.54×10^{-4} S cm^{-1} at ambient temperature which is an order of magnitude higher compared to that of the parent compound, $Mg_{0.5}Si_2(PO_4)_3$ as reported in [4]. This demonstrates that insertion Al^{3+} slightly increases the conductivity of this compound by producing additional interstitial Mg^{2+} ion which increases the number and mobility of ion.

Figure 6 presents the graph of *log σ(ac)* versus *log ω* for the $Mg_{0.5+x/2}Si_{2-x}Al_x(PO_4)_3$ (x = 0.10, 0.15, 0.20 and 0.25) samples. The plot can be divided into three regions; the low-frequency, intermediate frequency and high frequency regions. The spectra exhibit a spike in low-frequency region due to the polarization effects where the blocking of ions between the sample and electrode occurs. There is a plateau at the intermediate frequency region and extrapolating it to the y-axis gives the value of direct current conductivity, σ_{dc} [14-15]. In this region, the conductivity is frequency independent and the σ_{dc} values are found to be in good agreement with the value listed in Table 2. On the other hand, at high frequency region, the transition from direct current plateau to alternate current conductivity dispersion occurs.

According Almond and co-workers [16], the ionic hopping ω_p can be directly obtained from alternate currrent conductivity graph. The value of ionic hopping ω_p can be obtained by extrapolating, at twice the value of direct current conductivity, from the vertical axis horizontally towards the graph and then extrapolating downwards vertical to the horizontal axis as shown in

Figure 6. Using the ω_p value, the magnitude of the charge carrier concentration, K can be calculated using the equation as follows [17-18]:

$$K = \frac{\sigma T}{\omega_p} \quad (5)$$

$$K = ne^2a^2\gamma k^{-1} \quad (6)$$

where e is electron charge, γ is correlation factor which is set equal to 1, and a is the jump distance between two adjacent sites for the ions to hope that is assumed to be 3 Å [19]. The density of mobile ions (Mg^{2+}), n, can be determined using Eq. 6, and k is the Boltzmann constant. The ionic mobility, μ can be evaluated using Eq. 7 :

$$\mu = \frac{\sigma_{dc}}{ne} \quad (7)$$

The values of ω_p, K, n and μ at room temperature studied for $Mg_{0.5+x/2}Si_{2-x}Al_x(PO_4)_3$ compounds are presented in Table 3. The values of K, n and μ increase with the increase in x. This means that the rise in conductivity in the samples can be attributed to the extra Mg^{2+} interstitial ion which rise in ionic mobility as well as density of mobile ions [19-21].

Figure 7 depicts the dielectric constant (ε') versus log f for different x value of $Mg_{0.5+x/2}Si_{2-x}Al_x(PO_4)_3$ samples. At low frequency region, the value of ε' increases with the increase of x. This is due to the contribution of charge carrier accumulation at the interface of the sample and electrode [19-22]. This ε' value is greater than the value in parent compound, $Mg_{0.5}Si_2(PO_4)_3$ as reported in [4]. Its proving that, the substitutions of Al^{3+} at the Si^{4+} lattice site ($Si^{4+} \leftrightarrow Al^{3+} + 1/2Mg^{2+}$) affected the number of charge carrier in the sample.

Figure 8 shows the graph of dielectric loss (ε'') of $Mg_{0.5+x/2}Si_{2-x}Al_x(PO_4)_3$ as a function of log f at different value of x. The ε'' values also increase with the increases of x at low frequency

region. It's because, when the *x* value increase, the large amount of Mg^{2+} interstitial ions created. The increase of Mg^{2+} interstitial ions resulting high electrical energy loss due to the migration of ion to the surface of the sample which increase the value of *ε"*. [19-22].

Figure 9 presents the plot of frequency dependence of tan δ = *ε"*/ *ε'* at different *x*. The plot shows a peaking behavior for all *x*. As the *x* increases, the tan δ peaks are shifted toward higher frequency. The angular frequency ω ($\omega=2\pi f_{max}$) which corresponds to maximum tan δ gives the relaxation times τ, from the relation [21-22].

$$\omega_{max}\tau = 1 \qquad (10)$$

The relaxation times, τ is inversely proportional to jumping probability *P* which is expressed as [21-22]:

$$\tau = \frac{1}{2}P \qquad (11)$$

The τ for the samples with *x* = 0.10, 0.15, 0.20 and 0.25 are 1.71×10^3, 2.15×10^3, 4.28×10^3 and 4.28×10^4 Hz respectively. The results demonstrate that the ions in the sample *x* = 0.25 had the highest jumping probability. This value is higher compared to the τ value in parent compound, $Mg_{0.5}Si_2(PO_4)_3$ (3.8×10^4 Hz) as reported in [4]. Its demostared the extra Mg^{2+} interstitial ion affected the jumping probability of ions in the sample.

Linear sweep voltammetry was employed in this work to examine the decomposition voltage of the $Mg_{0.5+x/2}Si_{2-x}Al_x(PO_4)_3$ electrolyte samples. The linear sweep voltammogram of the $Mg_{0.5+x/2}Si_{2-x}Al_x(PO_4)_3$ sample with *x* = 0.25, which is the highest conducting compound is shown in Figure 10. The value of voltage stability window of the magnesium electrolyte is found

to be 2.51 V. This value is acceptable in magnesium battery since the potential difference between magnesium metal electrodes in less than 0.4 V [23].

4. CONCLUSION

The effects of Mg^{2+} interstitial ion on the properties of $Mg_{0.5+x/2}Si_{2-x}Al_x(PO_4)_3$ ceramic electrolytes were studied. The XRD result showed that Al^{3+} was successfully inserted into the parent $Mg_{0.5}Si_2(PO_4)_3$ since all the peaks were attributed only to this compound. Meanwhile, the conductivity study on room temperature showed an increasing pattern up to 1.54×10^{-4} S cm^{-1}. The conductivity parameters such as hopping frequencies, charge carrier concentration and mobile ion concentration proved that the increase in conductivity with *x* was due to the increase of Mg^{2+} interstitial ion . The $Mg_{0.5+x/2}Si_{2-x}Al_x(PO_4)_3$ sample exhibited a stable voltage window in voltage range of 2.51 V at ambient temperature.

ACKNOWLEDGEMENT

The authors would like to extend their gratitude towards the University of Malaya and Ministry of Education for funding this work through the Fundamental Research Grant Scheme (project no: FP006-2013B), University of Malaya Research Grant (project no: RP013A-13AFR), and Postgraduate Research Grant (project no: PG032- 2015A).

REFERENCES

[1] L. Dongping , X. Terrence, S. Partha, M. K Datta, M. L. Gordin, A. Manivannan, P.N. Kumta, D Wang, A Scientific Study of Current Collectors for Mg Batteries in Mg(AlCl2EtBu)2/THF Electrolyte, Journal of The Electrochemical Society, 160 (2) (2013), A351-A355.

[2] N. Anuar, S.B.R.S Adnan, N.S Mohamed, Characterization of $Mg_{0.5}$ $Zr_2(PO_4)_3$ for potential use as electrolyte in solid state magnesium batteries, Ceramics International, 40 (2014) 13719-13727.

[3] E. Levi, M. Levi, O. Chasid, D. Aurbach, A review on the problems of the solid state ions diffusion in cathodes for rechargeable Mg batteries, Journal of Electroceramics, 22 (2009) 13-19.

[4] Z.A Halim,S.B.R.S Adnan, N.S Mohamed, Effect of sintering temperature on the structural, electrical and electrochemical properties of novel $Mg_{0.5}Si_2(PO_4)_3$ ceramic electrolytes, Ceramics International, 42, (2016) 4452-4461.

[5] Z. Khakpour, influence of M: Ce^{4+}, Gd^{3+} and Yb^{3+} substituted $Na_{3+x}Zr_{2x}M_xSi_2PO_{12}$ solid NASICON electrolytes on sintering, microstructure and conductivity, Electrochimica Acta,196,(2016) 337-347.

[6] M. Illbeigi, A. Fazlali, M. Kazazi, A. H. Mohammadi, Effect of simultaneous addition of aluminum and chromium on the lithium ionic conductivity of $LiGe_2(PO_4)_3$ NASICON-type glass–ceramics, Solid State Ionics, 289 (2016) 180–187.

[7] S.B.R.S Adnan, F.M.Salleh, N.S Mohamed, Effect of interstitial Li+ ion and vacant site Li+ ion on the properties of novel Li2.05ZnAl0.05Si0.95O4 and Li1.95Zn0.95Cr0.05SiO4 ceramic electrolytes, Ceramics International, 42, 15(2016) 17941-17945.

[8] S.B.R.S Adnan, N.S Mohamed, Characterization of novel $Li_4 Zr_{0.06} Si_{0.94} O_4$ and $Li_{3.94} Cr_{0.02} Zr_{0.06} Si_{0.94} O_4$ ceramic electrolytes for lithium cells, Ceramics International, 40 (2014) 6373-6379.

[9] S.B.R.S Adnan, N. S Mohamed, Effects of Sn substitution on the properties of Li 4 SiO 4 ceramic electrolyte, Solid State Ionics, 262 (2014) 559-562.

[10] F. Wang, Y. Han, C.S. Lim, Y. Lu, J. Wang, J. Xu, H. Chen, C. Zhang, M. Hong, X. Liu, Simultaneous phase and size control of upconversion nanocrystals through lanthanide doping, Nature, 463 (2010) 1061-1065.

[11] C. Xu, J. Tamaki, N. Miura, N. Yamazoe, Grain size effects on gas sensitivity of porous SnO 2-based elements, Sensors and Actuators B: Chemical, 3 (1991) 147-155.

[12] R. Norhaniza, R. Subban, N.S Mohamed, Ion conduction in vanadium-substituted LiSn2P3O12 electrolyte nanomaterials, Journal of materials science, 46 (2011) 7815-7821.

[13] C. Mariappan, G. Govindaraj, Conductivity and ion dynamic studies in the Na 4.7+ x Ti 1.3− x (PO 4) 3.3− x (0≤ x≤ 0.6) NASICON material, Solid state ionics, 176 (2005) 1311-1318.

[14] E. Traversa, H. Aono, Y. Sadaoka, L. Montanaro, Electrical properties of sol–gel processed NASICON having new compositions, Sensors and Actuators B: Chemical, 65 (2000) 204-208.

[15] A. Orliukas, A. Dindune, Z. Kanepe, J. Ronis, B. Bagdonas, A. Kežionis, Synthesis and peculiarities of electric properties of Li 1.3 Zr 1.4 Ti 0.3 Al 0.3 (PO 4) 3 solid electrolyte ceramics, Electrochimica acta, 51 (2006) 6194-6198.

[16] D. Almond, G. Duncan, A. West, The determination of hopping rates and carrier concentrations in ionic conductors by a new analysis of ac conductivity, Solid State Ionics, 8 (1983) 159-164.

[17] R. Sobiestianskas, A. Dindune, Z. Kanepe, J. Ronis, A. Kežionis, E. Kazakevičius, A. Orliukas, Electrical properties of Li 1+ x Y y Ti 2− y (PO 4) 3 (where x, y= 0.3; 0.4) ceramics at high frequencies, Materials Science and Engineering: B, 76 (2000) 184-192.

[18] M. Prabu, S. Selvasekarapandian, A. Kulkarni, G. Hirankumar, A. Sakunthala, Ionic conductivity studies on LiSmO2 by impedance spectroscopy, Ionics, 16 (2010) 317-321.

[19] S.B.R.S Adnan, N.S Mohamed, Citrate sol-gel synthesised Li4SiO4: conductivity and dielectric behaviour, Materials Research Innovations, 16 (2012) 281-285.

[20] N. Hegab, A. Bekheet, M. Afifi, L. Wahaba, H. Shehata, Effect of Cd addition on the AC conductivity and dielectric properties of Ge 70 Te 30 films, Journal Ovonic Research, 3 (2007) 71-82.

[21] M. Vijayakumar, G. Hirankumar, M. Bhuvaneswari, S. Selvasekarapandian, Influence of B 2 O 3 doping on conductivity of LiTiO 2 electrode material, Journal of power sources, 117 (2003) 143-147.

[22] S.B.R.S Adnan, N.S Mohamed, Conductivity and dielectric Studies of Li_2ZnSiO_4 Ceramic Electrolyte Synthesized via Citrate Sol gel Method, International Journal of Electrochemical Science, International Journal of Electrochemical Science, 7 (2012) 9844-9858.

[23] R. Mohtadi, F. Mizuno, Magnesium batteries: Current state of the art, issues and future perspectives, Beilstein Journal of Nanotechnology, 5, (2014) 1291 – 1311

COVER LETTER FOR SUBMISSION MANUSCRIPT

Syed Bahari Ramadzan Syed Adnan,
Centre of foundation studies in sciences,
University of Malaya,
50603 Kuala Lumpur,
Malaysia

Subject: **SUBMISSION MASNUSCRIPT**

Dear Editor,

I'm closing herewith a manuscript entitled **"Effects of Mg^{2+} interstitial ion on the properties of $Mg_{0.5+x/2}Si_{2-x}Al_x(PO_4)_3$ ceramic electrolytes"** for publication in your journal.

Thank You.

Sincerely,
Syed Bahari Ramadzan Syed adnan, PhD

Figure 1

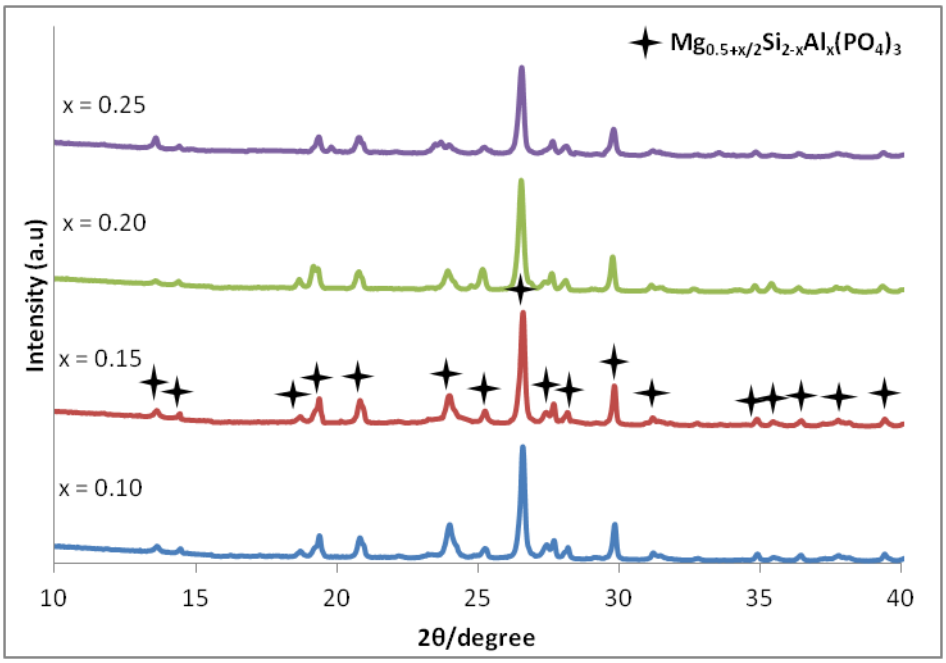

Figure 1: X-ray diffractograms $Mg_{0.5+x/2}Si_{2-x}Al_x(PO_4)_3$ samples

Figure 2

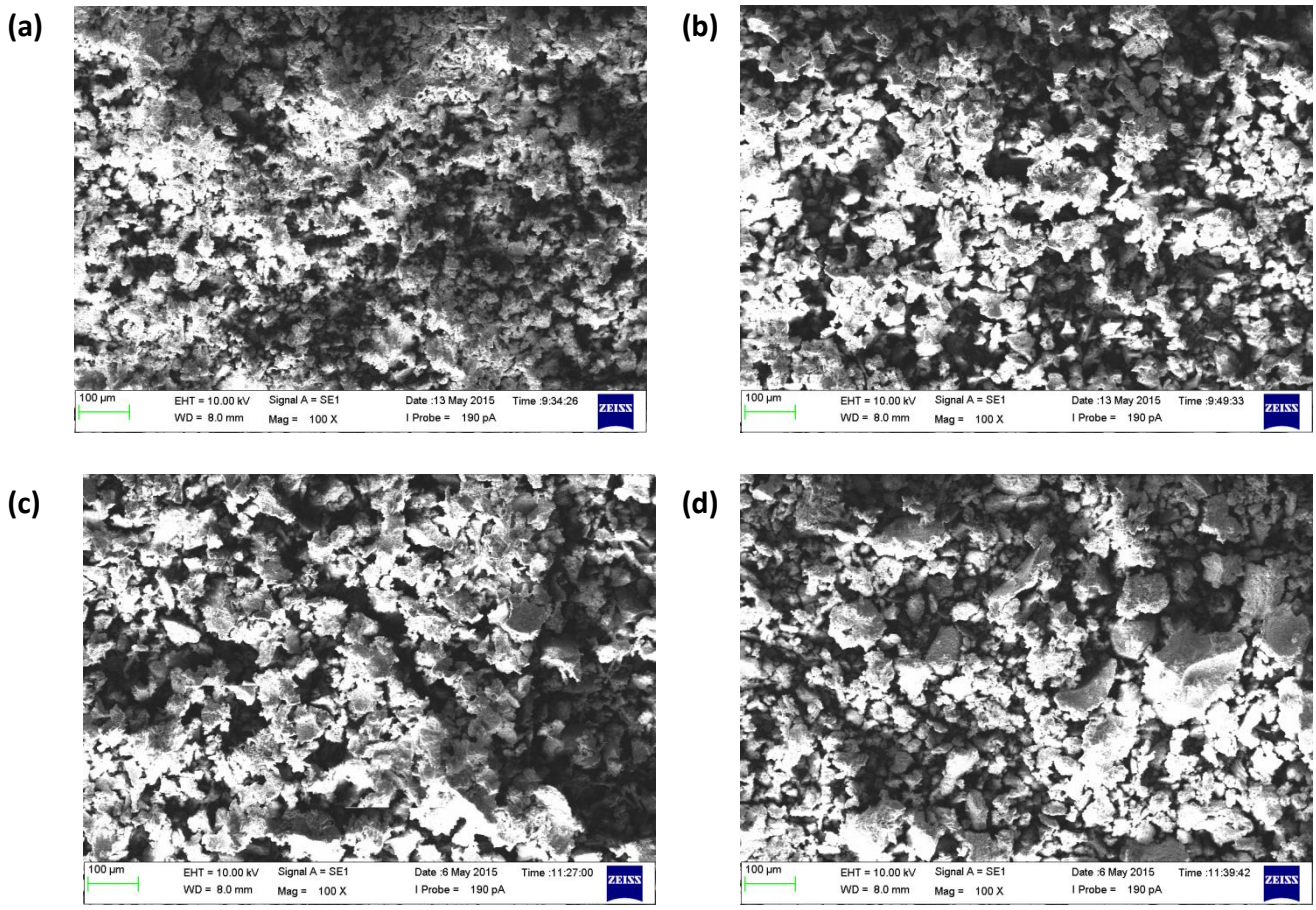

Figure 2: Cross-sectional SEM micrographs of the $Mg_{0.5+x/2}Si_{2-x}Al_x(PO_4)_3$ samples with (a) x = 0.10, (b) x = 0.15, (c) x = 0.20 and (d) x = 0.25

Figure 3

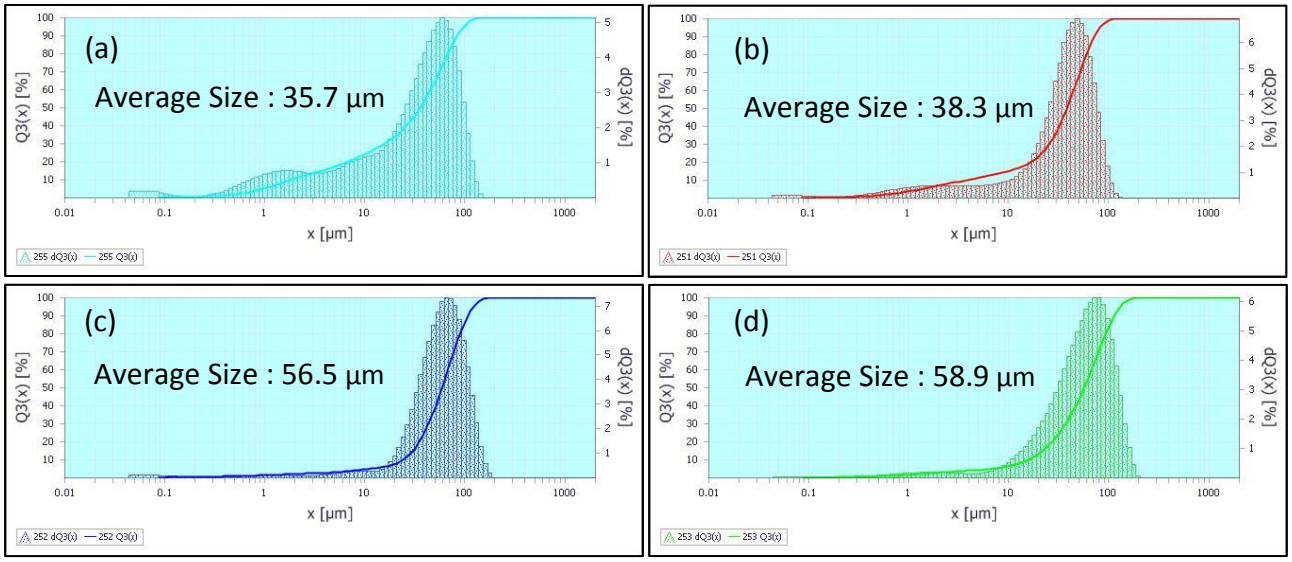

Figure 3: Particle size distribution of the $Mg_{0.5+x/2}Si_{2-x}Al_x(PO_4)_3$ samples with (a) x = 0.10, (b) x = 0.15, (c) x = 0.20 and (d) x = 0.25

Figure 4

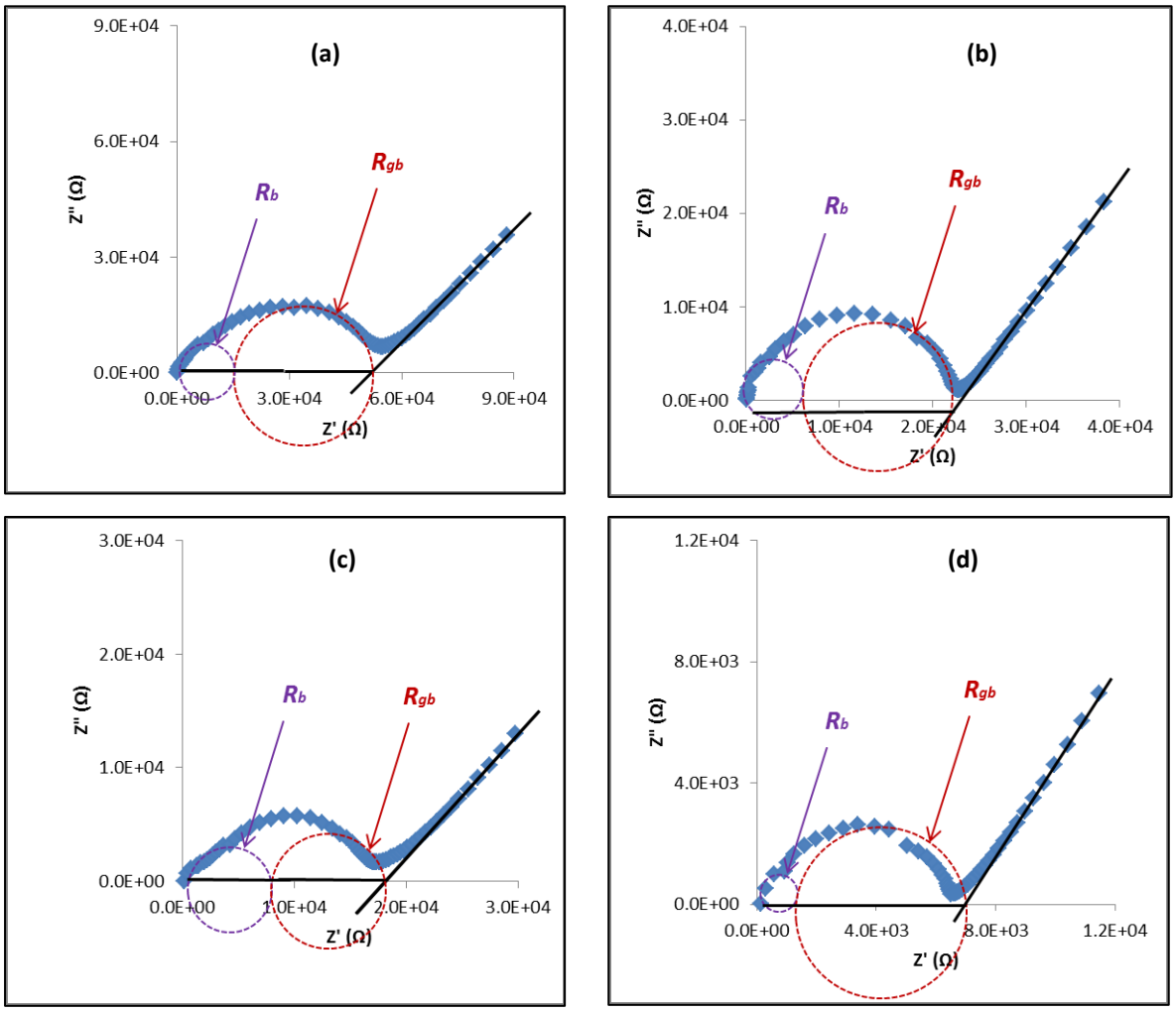

Figure 4: Typical complex impedance plots of the $Mg_{0.5+x/2}Si_{2-x}Al_x(PO_4)_3$ samples with (a) x = 0.10, (b) x = 0.15, (c) x = 0.20 and (d) x = 0.25

Figure 5

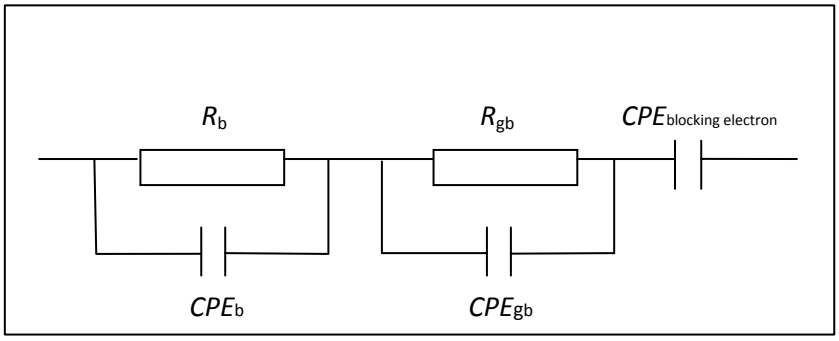

Figure 5: Equivalent circuit of $Mg_{0.5+x/2}Si_{2-x}Al_x(PO_4)_3$ samples based on the impedance analysis of the samples at room temperature

Figure 6

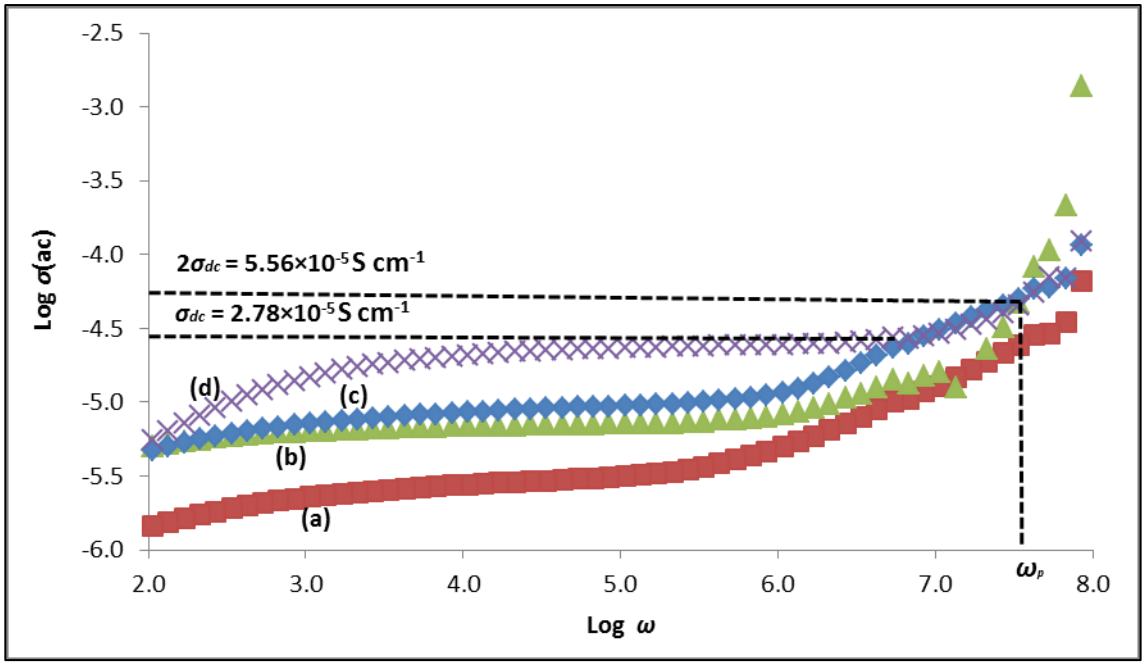

Figure 6: Alternate current conductivity spectra of the $Mg_{0.5+x/2}Si_{2-x}Al_x(PO_4)_3$ samples with (a) x = 0.10, (b) x = 0.15, (c) x = 0.20 and (d) x = 0.25

Figure 7

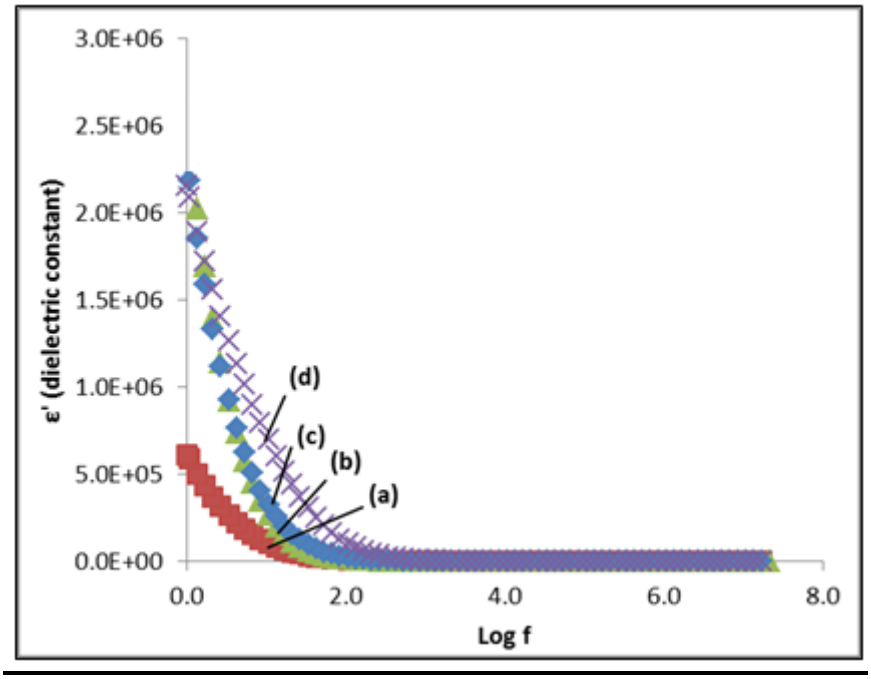

Figure 7: Plot of dielectric constant (ε') as a function of log *f* of the $Mg_{0.5+x/2}Si_{2-x}Al_x(PO_4)_3$ samples with (a) x = 0.10, (b) x= 0.15, (c) x = 0.20 and (d) x = 0.25

Figure 8

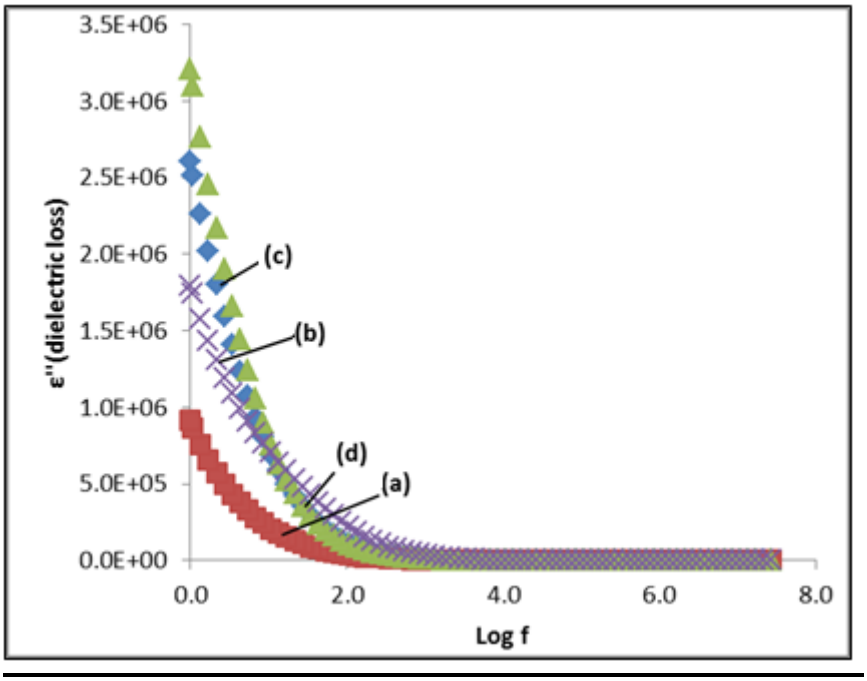

Figure 8: Plot of dielectric loss (ε'') as a function of log f for the $Mg_{0.5+x/2}Si_{2-x}Al_x(PO_4)_3$ samples with (a) x = 0.10, (b) x = 0.15, (c) x = 0.20 and (d) x = 0.25

Figure 9

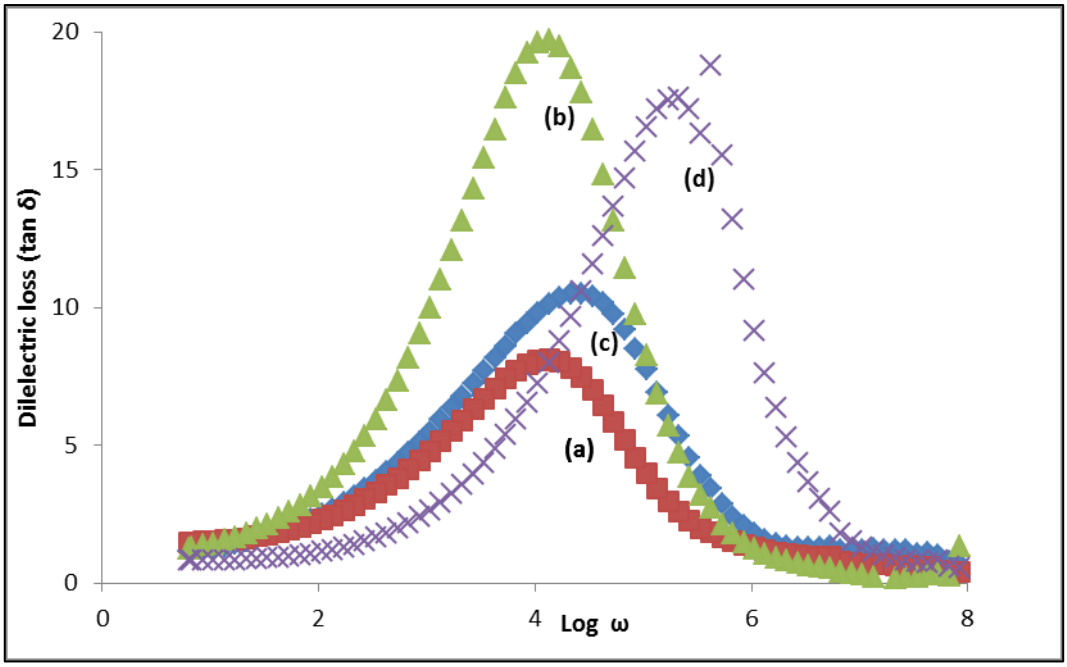

Figure 9: Frequency dependence of tan δ for the $Mg_{0.5+x/2}Si_{2-x}Al_x(PO_4)_3$ samples with (a) x = 0.10, (b) x = 0.15, (c) x = 0.20 and (d) x = 0.25

Figure 10

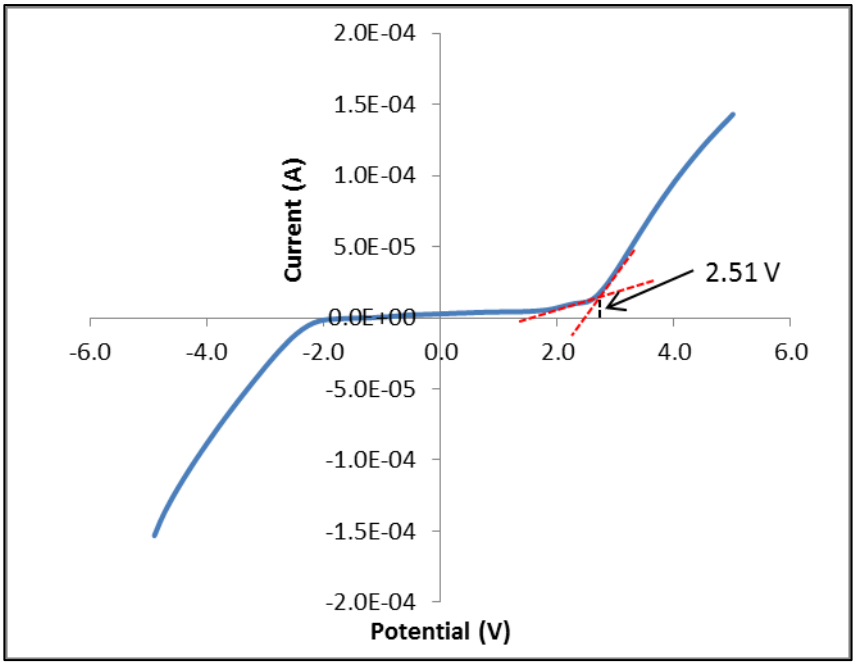

Figure 10: Linear sweep voltammogram of the $Mg_{0.5+x/2}Si_{2-x}Al_x(PO_4)_3$ samples with x = 0.25 with a sweep rate of 50 mV s^{-1}

Table 1

Table 1: Lattice parameters, unit cell volume, crystallite size and density of $Mg_{0.5+x/2}Si_{2-x}Al_x(PO_4)_3$ samples

Samples	*α*(Å)	*b* (Å)	*c* (Å)	*V* (Å^3)	Crystallite size (Å)
***x* = 0.10**	6.707	5.750	12.433	479.496	86.299
***x* = 0.15**	6.720	5.755	12.456	481.687	115.100
***x* = 0.20**	6.733	5.764	12.501	485.172	115.100
***x* = 0.25**	6.740	5.774	12.524	487.327	138.099

Table 2: The σ_b, σ_{gb} and σ_t of $Mg_{0.5+x/2}Si_{2-x}Al_x(PO_4)_3$ samples at ambient temperature

Sample	***x***	σ_b **(S cm^{-1})**	σ_{gb} **(S cm^{-1})**	σ_t **(S cm^{-1})**
$\mathbf{Mg_{0.5+x/2}Si_{2-x}Al_x(PO_4)_3}$	0.10	1.27×10^{-5}	5.11×10^{-6}	3.65×10^{-6}
	0.15	2.94×10^{-5}	1.17×10^{-5}	8.37×10^{-6}
	0.20	2.52×10^{-5}	1.86×10^{-5}	1.07×10^{-5}
	0.25	1.54×10^{-4}	3.39×10^{-5}	2.78×10^{-5}

Table 3: Value of ω_p, K, n and μ at room temperatures for $Mg_{0.5+x/2}Si_{2-x}Al_x(PO_4)_3$ samples

Sample	ω_p **(Hz)**	K **(S cm^{-1} K Hz^{-1})**	$n\times10^{23}$ **(cm^{-3})**	μ **(cm^2 V^{-1} s^{-1})**
x = 0.10	2.69×10^{6}	4.11×10^{-10}	1.54	1.48×10^{-10}
x = 0.15	3.39×10^{6}	7.48×10^{-10}	2.80	1.87×10^{-10}
x = 0.20	4.27×10^{6}	7.60×10^{-10}	2.84	2.35×10^{-10}
x = 0.25	2.27×10^{7}	7.97×10^{-10}	7.39	2.35×10^{-09}